Cycle Slip Detection and Fixing by MEMS-IMU/GPS Integration for Mobile Environment RTK-GPS

Tomoji Takasu, Akio Yasuda
Tokyo University of Marine Science and Technology, Japan

BIOGRAPHY

Tomoji Takasu is a researcher in Funai Laboratory of Satellite Navigation at Tokyo University of Marine Science and Technology. He was working for developments of satellite systems at NEC Aerospace systems Ltd. from 1984 to 1997. He is currently involved in the research and development of precise positioning algorithms with GPS/GNSS, including PPP, RTK-GPS and INS/GPS integration.

Akio Yasuda graduated in 1966 from Dept. of Electrical Eng., Nagoya Institute of Technology, and obtained Dr. of Eng. degree from Nagoya University, and worked at Nagoya University and at Tokyo University of Mercantile Marine. Since 2004, he was Prof. at Tokyo University of Marine Science and Technology. He is currently conductor of Funai laboratory of Satellite Navigation. He was engaged in research on development of marine wave meter, BS and GMS reception onboard, regional positioning system with geostationary satellites. His concerning of GPS started in 1987. He is presently conducting the researches on multipath mitigation, analysis of ionospherical delay, improvement of RTK-GPS algorism, and the other GPS related subjects. He is a member of IEICE (fellow), Japan Inst. Navigation, ION and IEEE.

ABSTRACT

The performance of the mobile environment RTK-GPS in urban areas is much degraded compared to the good condition under the open sky. One of the reasons for the degradation is cycle slips. The cycle slip forces discontinuity of integer ambiguity and worsens the condition of carrier-based positioning. To improve these conditions, it is effective to integrate INS to GPS. For RTK-GPS of mobile vehicles, INS can be used for the cycle slip detection and fixing. We propose a simple integration scheme of INS/GPS and RTK-GPS with a low-cost MEMS-IMU for the purpose. We conducted the field test to verify and evaluate the performance of the scheme. According to the results of the experiment, the scheme works effectively in the severe condition with many cycle slips.

INTRODUCTION

RTK-GPS (real-time kinematic GPS) is one of the most precise positioning technologies, with which users can obtain cm-level accuracy of the position in real-time by processing carrier-phase measurements of GPS/GNSS signals. RTK-GPS has already been utilized for many applications like land survey, construction, agriculture and transportation. Recently, some researchers tried to apply RTK-GPS to precise navigation of mobile vehicles. In good condition, under the open sky and with many visible satellites, RTK-GPS provides fair performance even in such mobile environment. However, in severe situations like when driving on a downtown street in an urban canyon, the performance becomes very poor. It indicates much more outages of solutions, worse accuracy and lower fix-rate. One reason for the performance degradation in such condition is cycle slips. A cycle slip is a sudden jump of carrier-phase measurements by loss-of-lock of signal tracking. The cycle slip forces discontinuity of integer ambiguity and worsens the condition of carrier-based positioning. Furthermore, much more cycle slips occur in mobile environment than in static condition. One of the major technical issues for mobile environment RTK-GPS in urban areas is to overcome the cycle slips.

For mobile vehicle navigation, INS (inertial navigation system) is often integrated with GPS/GNSS to improve the performance. In such an INS/GPS integrated system, INS is mainly used to obtain user positions and velocities during GPS signal outage. For mobile environment RTK-GPS, this INS/GPS integration is also effective to improve the positioning condition with many cycle slips. In this study, we try to integrate a low-cost MEMS (micro electro mechanical systems) IMU (inertial measurement unit) into the RTK-GPS navigation in order to detect and repair the cycle slips. A simple integration scheme is proposed to combine GPS/GNSS and INS measurements.

The result of a field experiment is also presented to verify and evaluate the proposed scheme.

CYCLE SLIP

A cycle slip is defined as a discontinuity in carrier-phase measurements caused by loss-of-lock of signal tracking in a GPS/GNSS receiver [1]. With a cycle slip, a jump of integer number of cycles (or plus a half cycle) appears in carrier-phase ambiguity. Most of the cycle slips are caused by signal obstruction due to surrounding obstacles, like buildings, trees, bridges, poles, cars, so on. Therefore, far more slips are shown in mobile environment compared to in stationary condition. Figure 1 shows the example of cycle slips when driving on a street in an urban canyon. The red lines indicate cycle slips in this figure.

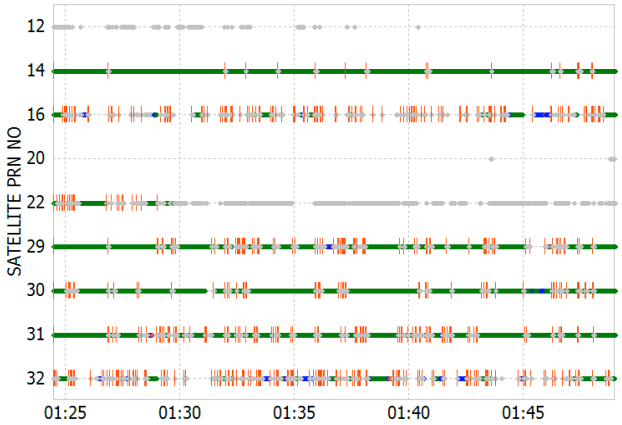

Figure 1. Example of cycle slips in urban areas

Figure 2 shows a typical cycle slip pattern. Valid carrier-phase measurements are expressed as green points. Once an obstacle block GPS/GNSS signal, the GPS/GNSS receiver loose the lock of carrier tracking due to the weak signal level. Signal outages and data gaps are often involved in this period. When the receiver moves and the signal recovered, a reacquisition process runs to recover the tracking in the receiver. Typically, it takes about 1 second. A cycle slip appears at this time. In the most receivers, a half-cycle ambiguity resolution step follows. At the maximum, it takes 12 seconds, that is two sub-frame cycles of navigation messages, to recover the normal tracking even after very short signal outage. In this period, the proper carrier-phase measurements are not available. Furthermore, once a cycle slip detected, the most RTK-GPS receivers just reinitialize and restart the estimated carrier-phase ambiguity. It often takes minutes in severe condition. Therefore, with frequent cycle slips, the availability of precise solutions becomes very low. Additionally, it is not easy to recognize a small cycle slip properly in mobile condition. A miss-detection of a cycle slip much degrades the accuracy. Reliable detection of cycle slips is more important in these situations.

Figure 3 shows a histogram of the data gaps with cycle slips in the same condition as Figure 1. In this example, most of the data gaps are shorter than 10 seconds. With such short data gaps, INS might aid receivers effectively to recover the cycle slips. If the slips were fixed, the performance of RTK-GPS would be much improved in severe conditions.

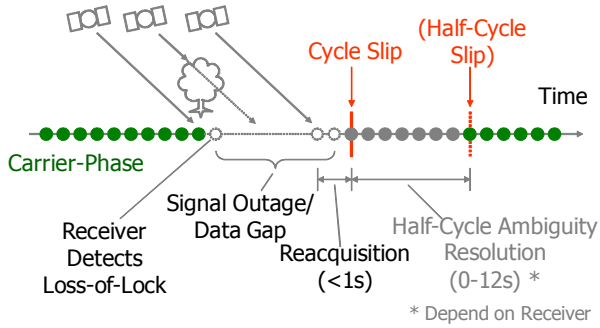

Figure 2. Typical cycle slip pattern

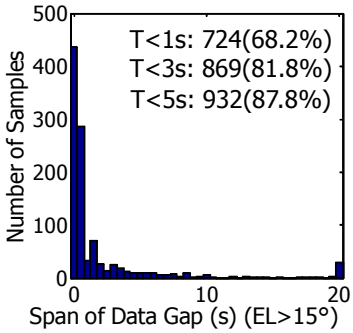

Figure 3. Histogram of data gaps with cycle slips in urban areas

RTK-GPS FORMULATIONS

By using EKF (extended Kalman filter) [2], a state vector $\boldsymbol{x}$ and its covariance matrix $\boldsymbol{P}$ can be estimated with a measurement vector $\boldsymbol{y}_k$ at an epoch t_k by:

$$\begin{aligned}
&\hat{\boldsymbol{x}}_k(+) = \hat{\boldsymbol{x}}_k(-) + \boldsymbol{K}_k(\boldsymbol{y}_k - \boldsymbol{h}(\hat{\boldsymbol{x}}_k(-))) \\
&\boldsymbol{P}_k(+) = (\boldsymbol{I} - \boldsymbol{K}_k\boldsymbol{H}(\hat{\boldsymbol{x}}_k(-)))\boldsymbol{P}_k(-) \\
&\boldsymbol{K}_k = \boldsymbol{P}_k(-)\boldsymbol{H}(\hat{\boldsymbol{x}}_k(-))(\boldsymbol{H}(\hat{\boldsymbol{x}}_k(-))\boldsymbol{P}_k(-)\boldsymbol{H}(\hat{\boldsymbol{x}}_k(-))^T + \boldsymbol{R}_k)^{-1}
\end{aligned} \tag{1}$$

where $\boldsymbol{h}(\boldsymbol{x})$, $\boldsymbol{H}(\boldsymbol{x})$ and $\boldsymbol{R}_k$ are the measurements model vector, the matrix of partial derivatives and the covariance matrix of measurement errors, respectively. Assuming the system-model linear, the time update of the state vector and its covariance by EKF is expressed as:

$$\begin{aligned}
&\hat{\boldsymbol{x}}_{k+1}(-) = \boldsymbol{F}_k^{k+1}\hat{\boldsymbol{x}}_k(+) \\
&\boldsymbol{P}_{k+1}(-) = \boldsymbol{F}_k^{k+1}\boldsymbol{P}_k(+)\boldsymbol{F}_k^{k+1^T} + \boldsymbol{Q}_k^{k+1}
\end{aligned} \tag{2}$$

where:

$\boldsymbol{F}_k^{k+1}$: state transition matrix from t_k to t_{k+1}

$\boldsymbol{Q}_k^{k+1}$: covariance matrix of system noise

For carrier-based relative positioning with a short length baseline between the rover r and the base-station b, the following measurement equations are commonly used. In these equations, the satellite and receiver clock biases, and the atmospheric effects are eliminated by using double-differencing technique.

$$\begin{aligned} \Phi_{rb}^{ij} &\equiv \lambda\phi_{rb}^{ij} = \rho_{rb}^{ij} + \lambda(N_{rb}^{i} - N_{rb}^{j}) + \varepsilon_{\Phi} \\ P_{rb}^{ij} &= \rho_{rb}^{ij} + \varepsilon_{P} \end{aligned} \tag{3}$$

where:

$()^{ij}$: single-difference between satellite i and j

$()_{rb}$: single-difference between receiver r and b

ϕ_r^i : carrier-phase measurement (cycle)

P_r^i : pseudorange measurement (m)

ρ_r^i : geometric range (m)

λ : carrier wave length (m)

N_r^i : carrier-phase ambiguity (cycle)

ε_{Φ} , ε_P : measurement errors of carrier-phase and pseudorange (m)

Assuming the use of dual-frequency GPS/GNSS receivers for both of the rover and the base-station, the unknown state vector $\boldsymbol{x}$ for RTK-GPS positioning is defined as:

$$\boldsymbol{x} = (\boldsymbol{r}_r^{\,T}, \boldsymbol{v}_r^{\,T}, \boldsymbol{N}_{L1}^{\,T}, \boldsymbol{N}_{L2}^{\,T})^T \tag{4}$$

where:

$\boldsymbol{r}_r$: rover antenna position (ECEF) (m)

$\boldsymbol{v}_r$: rover antenna velocity (ECEF) (m/s)

$\boldsymbol{N}_{Lj} = (N_{rb,Lj}^1, N_{rb,Lj}^2, ..., N_{rb,Lj}^m)^T$: single-differences of L_j carrier-phase ambiguities (cycle)

Note that single-difference is used instead of double-difference for carrier-phase ambiguities to avoid the hand-over problem of reference satellites. The measurement vector $\boldsymbol{y}_k$ is also defined with double-differenced carrier-phase and pseudorange measurements as:

$$\begin{aligned} \boldsymbol{y}_k &= (\boldsymbol{\Phi}_{L1,}^{\,T}, \boldsymbol{\Phi}_{L2,}^{\,T}, \boldsymbol{P}_{L1}^{\,T}, \boldsymbol{P}_{L2}^{\,T})^T \\ \boldsymbol{\Phi}_{Lj} &= (\Phi_{rb,Lj}^{12}, \Phi_{rb,Lj}^{13}, \Phi_{rb,Lj}^{14}, ..., \Phi_{rb,Lj}^{1m})^T \\ \boldsymbol{P}_{Lj} &= (P_{rb,Lj}^{12}, P_{rb,Lj}^{13}, P_{rb,Lj}^{14}, ..., P_{rb,Lj}^{1m})^T \end{aligned} \tag{5}$$

By using equation (3), the measurement model vector $\boldsymbol{h}(\boldsymbol{x})$ and the matrix of partial derivatives $\boldsymbol{H}(\boldsymbol{x})$ can be written as:

$$\boldsymbol{h}(\hat{\boldsymbol{x}}) = (\boldsymbol{h}_{\Phi,L1}^{\,T}, \boldsymbol{h}_{\Phi,L2}^{\,T}, \boldsymbol{h}_{P,L1}^{\,T} \boldsymbol{h}_{P,L2}^{\,T})^T \tag{6}$$

$$\boldsymbol{h}_{\Phi,Lj} = \begin{pmatrix} \rho_{rb}^{12} + \lambda_{Lj}(\hat{N}_{rb}^1 - \hat{N}_{rb}^2) \\ \rho_{rb}^{13} + \lambda_{Lj}(\hat{N}_{rb}^1 - \hat{N}_{rb}^3) \\ \vdots \\ \rho_{rb}^{1m} + \lambda_{Lj}(\hat{N}_{rb}^1 - \hat{N}_{rb}^m) \end{pmatrix}, \boldsymbol{h}_{P,Lj} = \begin{pmatrix} \rho_{rb}^{12} \\ \rho_{rb}^{13} \\ \vdots \\ \rho_{rb}^{1m} \end{pmatrix}$$

$$\rho_r^i = \left\| \hat{\boldsymbol{r}}_r - \boldsymbol{r}^i \right\|, \rho_b^i = \left\| \boldsymbol{r}_b - \boldsymbol{r}^i \right\|$$

$$\boldsymbol{H}(\hat{\boldsymbol{x}}) = \left.\frac{\partial \boldsymbol{h}(\boldsymbol{x})}{\partial \boldsymbol{x}}\right|_{\boldsymbol{x}=\hat{\boldsymbol{x}}} = \begin{pmatrix} -\boldsymbol{DE} & \boldsymbol{0} & \lambda_{L1}\boldsymbol{D} & \boldsymbol{0} \\ -\boldsymbol{DE} & \boldsymbol{0} & \boldsymbol{0} & \lambda_{L2}\boldsymbol{D} \\ -\boldsymbol{DE} & \boldsymbol{0} & \boldsymbol{0} & \boldsymbol{0} \\ -\boldsymbol{DE} & \boldsymbol{0} & \boldsymbol{0} & \boldsymbol{0} \end{pmatrix} \tag{7}$$

$$\boldsymbol{E} = (\boldsymbol{e}_r^1, \boldsymbol{e}_r^2, ..., \boldsymbol{e}_r^m)^T$$

where:

$\boldsymbol{r}^i$: satellite i position (ECEF) (m)

$\boldsymbol{r}_b$: base-station antenna position (ECEF) (m)

$\boldsymbol{e}_r^i$: LOS (line-of-sight) vector from rover antenna to satellite i

$$\boldsymbol{D} = \begin{pmatrix} 1 & -1 & 0 & \cdots & 0 \\ 1 & 0 & -1 & \cdots & 0 \\ \vdots & \vdots & \vdots & \ddots & \vdots \\ 1 & 0 & 0 & \cdots & -1 \end{pmatrix}$$: single-differencing matrix

The covariance matrix of the double-differenced measurement errors is also expressed as:

$$\boldsymbol{R}_k = \begin{pmatrix} \boldsymbol{D}\boldsymbol{R}_{\Phi,L1}\boldsymbol{D}^T & & & \\ & \boldsymbol{D}\boldsymbol{R}_{\Phi,L2}\boldsymbol{D}^T & & \\ & & \boldsymbol{D}\boldsymbol{R}_{P,L1}\boldsymbol{D}^T & \\ & & & \boldsymbol{D}\boldsymbol{R}_{P,L2}\boldsymbol{D}^T \end{pmatrix} \tag{8}$$

$$\boldsymbol{R}_{\Phi,Lj} = \mathrm{diag}(2\sigma_{\Phi,Lj}^{1\,2}, 2\sigma_{\Phi,Lj}^{2\,2}, ..., 2\sigma_{\Phi,Lj}^{m\,2})$$

$$\boldsymbol{R}_{P,Lj} = \mathrm{diag}(2\sigma_{P,Lj}^{1\,2}, 2\sigma_{P,Lj}^{2\,2}, ..., 2\sigma_{P,Lj}^{m\,2})$$

where:

$\sigma_{\Phi,Lj}^i$, $\sigma_{P,Lj}^i$: standard deviation of L_j carrier-phase and pseudorange measurement error (m)

For conventional RTK-GPS without INS, the time update of EKF is expressed by equation (2) with:

$$\boldsymbol{F}_k^{k+1} = \begin{pmatrix} \boldsymbol{I}_3 & \boldsymbol{I}_3\tau_r & & \\ & \boldsymbol{I}_3 & & \\ & & \boldsymbol{I}_{m-1} & \\ & & & \boldsymbol{I}_{m-1} \end{pmatrix}, \boldsymbol{Q}_k^{k+1} = \begin{pmatrix} \boldsymbol{0} & & & \\ & \boldsymbol{q}_v & & \\ & & \boldsymbol{0} & \\ & & & \boldsymbol{0} \end{pmatrix} \tag{9}$$

$$\boldsymbol{q}_v = \boldsymbol{E}_{enu-ecef}\,\mathrm{diag}(\sigma_{ve}^{\,2}\tau_r, \sigma_{vn}^{\,2}\tau_r, \sigma_{vu}^{\,2}\tau_r)\boldsymbol{E}_{enu-ecef}^{\,T}$$

where:

$\tau_r = t_{k+1} - t_k$: GPS/GNSS receiver sampling interval (s)

$\boldsymbol{E}_{enu-ecef}$: transformation matrix from local ENU coordinates to ECEF

$\sigma_{ve}, \sigma_{vn}, \sigma_{vu}$: standard deviations of east, north and up component of the rover velocity system noise (m/s/$\sqrt{\text{s}}$)

By solving the EKF formula (1), (2) with the RTK-GPS equation (4)-(9), the estimated rover antenna position, velocity and float carrier-phase ambiguities can be obtained.

AMBIGUITY RESOLUTION

Once estimated states obtained, the float carrier-phase ambiguities should be resolved into integer values in order to improve accuracy and convergence time. At first, the float solution and the covariance matrix are transformed to double-differenced forms by:

$$\begin{aligned} \hat{\boldsymbol{x}}'_k &= \boldsymbol{G}\,\hat{\boldsymbol{x}}_k(+) = (\hat{\boldsymbol{r}}_r{}^T, \hat{\boldsymbol{v}}_r{}^T, \hat{\boldsymbol{N}}^T)^T \\ \boldsymbol{P}'_k &= \boldsymbol{G}\boldsymbol{P}_k(+)\boldsymbol{G}^T = \begin{pmatrix} \boldsymbol{Q}_R & \boldsymbol{Q}_{NR} \\ \boldsymbol{Q}_{RN} & \boldsymbol{Q}_N \end{pmatrix} \end{aligned} \tag{10}$$

$$\boldsymbol{G} = \begin{pmatrix} \boldsymbol{I}_6 & & \\ & \boldsymbol{D} & \\ & & \boldsymbol{D} \end{pmatrix}$$

In this forms, the best integer vector $\breve{\boldsymbol{N}}$ for the double-differenced carrier-phase ambiguities is searched to satisfy the condition of ILS (integer least square) problem as:

$$\breve{\boldsymbol{N}} = \underset{\boldsymbol{N}\in\boldsymbol{Z}}{\operatorname{argmin}}\left((\boldsymbol{N}-\hat{\boldsymbol{N}})^T\,\boldsymbol{Q}_N{}^{-1}(\boldsymbol{N}-\hat{\boldsymbol{N}})\right) \tag{11}$$

To solve the problem, a well-known efficient strategy LAMBDA [3] and its extension MLAMBDA [4] are employed in this study. After the validation by the simple ratio-test, the fixed solution of the rover antenna position and velocity $\breve{\boldsymbol{r}}_r, \breve{\boldsymbol{v}}_r$ are obtained by solving the following equation.

$$\begin{pmatrix} \breve{\boldsymbol{r}}_r \\ \breve{\boldsymbol{v}}_r \end{pmatrix} = \begin{pmatrix} \hat{\boldsymbol{r}}_r \\ \hat{\boldsymbol{v}}_r \end{pmatrix} - \boldsymbol{Q}_{RN}\boldsymbol{Q}_N{}^{-1}(\hat{\boldsymbol{N}} - \breve{\boldsymbol{N}}) \tag{12}$$

INS NAVIGATION AND INS/GPS INTEGRATION

The INS navigation process is written as the following equations to updates attitude, velocity and position with the measurements of IMU [5]. In these formulas, the coordinates are expressed in the INS body frame (b-frame) and the ECEF frame (e-frame).

$$\boldsymbol{C}_b^e(+) = \boldsymbol{C}_b^e(-)\boldsymbol{C}_{b+}^{b-} - \boldsymbol{\Omega}_e\,\boldsymbol{C}_b^e(-)\,\tau_{ins} \tag{13}$$

$$\boldsymbol{C}_{b+}^{b-} = \boldsymbol{I}_3 + \sin\alpha\,(\boldsymbol{\alpha}\times)/\alpha + (1-\cos\alpha)(\boldsymbol{\alpha}\times)^2/\alpha^2$$

$$\boldsymbol{\alpha} = \boldsymbol{\omega}\,\tau_{ins}, \quad \alpha = \left\|\boldsymbol{\alpha}\right\|$$

$$\boldsymbol{v}_{ins}(+) = \boldsymbol{v}_{ins}(-) + (\boldsymbol{f}_e + \boldsymbol{g}(\boldsymbol{r}_{ins}(-)) - 2\boldsymbol{\Omega}_e\boldsymbol{v}_{ins}(-))\,\tau_{ins} \tag{14}$$

$$\boldsymbol{f}_e = (\boldsymbol{C}_b^e(-) + \boldsymbol{C}_b^e(+))\,\boldsymbol{f}/2$$

$$\boldsymbol{r}_{ins}(+) = \boldsymbol{r}_{ins}(-) + (\boldsymbol{v}_{ins}(-) + \boldsymbol{v}_{ins}(+))\,\tau_{ins}/2 \tag{15}$$

where:

$\boldsymbol{C}_b^e$: INS attitude as the transformation matrix from b-frame to e-frame

$\boldsymbol{r}_{ins}$: INS position (ECEF) (m)

$\boldsymbol{v}_{ins}$: INS velocity (ECEF) (m/s)

$\boldsymbol{\Omega}_e$: skew-symmetric matrix of the earth rotation

$\boldsymbol{\omega}$: angular rate measurements of gyroscopes (rad/s)

$\boldsymbol{f}$: specific force measurements of accelerometers (m/s^2)

$\boldsymbol{g}(\boldsymbol{r})$: gravity force at position $\boldsymbol{r}$ (m/s^2)

τ_{ins} : sampling interval of IMU (s)

According the standard INS/GPS integration scheme, the state vector $\boldsymbol{x}$ is defined as:

$$\boldsymbol{x} = (\delta\boldsymbol{\psi}_{ins}{}^T, \delta\boldsymbol{r}_{ins}{}^T, \delta\boldsymbol{v}_{ins}{}^T, \boldsymbol{b}_a{}^T, \boldsymbol{b}_g{}^T)^T \tag{16}$$

where:

$\delta\boldsymbol{\psi}_{ins}$: INS attitude correction (rad)

$\delta\boldsymbol{r}_{ins}$: INS position correction (ECEF) (m)

$\delta\boldsymbol{v}_{ins}$: INS velocity correction (ECEF) (m/s)

$\boldsymbol{b}_a$: accelerometer biases (m/s^2)

$\boldsymbol{b}_g$: gyroscope biases (rad/s)

The measurement vector $\boldsymbol{y}_k$ for the tightly coupled INS/GPS integration is expressed with single-differenced pseudorange P_r^{ij} and delta-range P_r^{ij} as:

$$\boldsymbol{y}_k = (P_{r,L1}^{12}, P_{r,L1}^{13}, ..., P_{r,L1}^{1m}, \dot{P}_{r,L1}^{12}, \dot{P}_{r,L1}^{13}, ..., \dot{P}_{r,L1}^{1m}) \tag{17}$$

The measurement model and the matrix of partial derivatives are also written with the INS navigation solution as:

$$\begin{aligned} \hat{\boldsymbol{C}}_b^e &= (\boldsymbol{I}_3 - \delta\hat{\boldsymbol{\psi}}_{ins}\times)\boldsymbol{C}_b^e \\ \hat{\boldsymbol{r}}_{ins/gps} &= \boldsymbol{r}_{ins} + \delta\hat{\boldsymbol{r}}_{ins} + \hat{\boldsymbol{C}}_b^e\boldsymbol{l}_r \\ \hat{\boldsymbol{v}}_{ins/gps} &= \boldsymbol{v}_{ins} + \delta\hat{\boldsymbol{v}}_{ins} + \hat{\boldsymbol{C}}_b^e(\boldsymbol{\omega}\times\boldsymbol{l}_r) + \boldsymbol{\Omega}_e\hat{\boldsymbol{C}}_b^e\boldsymbol{l}_r \\ \rho_r^i &= \left\|\hat{\boldsymbol{r}}_{ins/gps} - \boldsymbol{r}^i\right\|, \ \dot{\rho}_r^i = \left\|\hat{\boldsymbol{v}}_{ins/gps} - \boldsymbol{v}^i\right\| \end{aligned} \tag{18}$$

$$\boldsymbol{h}(\hat{\boldsymbol{x}}) = (\boldsymbol{h}_P(\hat{\boldsymbol{x}})^T, \boldsymbol{h}_{\dot{P}}(\hat{\boldsymbol{x}})^T)^T \tag{19}$$

$$\boldsymbol{h}_P(\hat{\boldsymbol{x}}) = \begin{pmatrix} \rho_r^{12} - cdT^{12} \\ \rho_r^{13} - cdT^{13} \\ \vdots \\ \rho_r^{1m} - cdT^{1m} \end{pmatrix}, \boldsymbol{h}_{\dot{P}}(\hat{\boldsymbol{x}}) = \begin{pmatrix} \dot{\rho}_r^{12} - cd\dot{T}^{12} \\ \dot{\rho}_r^{13} - cd\dot{T}^{13} \\ \vdots \\ \dot{\rho}_r^{1m} - cd\dot{T}^{1m} \end{pmatrix}$$

$$\boldsymbol{H}(\hat{\boldsymbol{x}}) = \left.\frac{\partial \boldsymbol{h}(\boldsymbol{x})}{\partial \boldsymbol{x}}\right|_{\boldsymbol{x}=\hat{\boldsymbol{x}}} = \begin{pmatrix} \boldsymbol{0} & -\boldsymbol{DE} & \boldsymbol{0} & \boldsymbol{0} & \boldsymbol{0} \\ \boldsymbol{0} & \boldsymbol{0} & -\boldsymbol{DE} & \boldsymbol{0} & \boldsymbol{0} \end{pmatrix} \tag{20}$$

where:

$\hat{\boldsymbol{C}}_b^e$: corrected attitude

$\hat{\boldsymbol{r}}_{ins/gps}$: corrected rover antenna position (ECEF) (m)

$\hat{\boldsymbol{v}}_{ins/gps}$: corrected rover antenna velocity (ECEF) (m/s)

$\boldsymbol{l}_r$: lever arm vector of rover antenna (m)

$\dot{\rho}_r^i$: range rate between rover antenna and satellite i (m/s)

$\boldsymbol{v}^i$: velocity of satellite i (ECEF) (m/s)

$dT^i, d\dot{T}^i$: satellite clock-bias and clock-drift of satellite i (s, s/s)

By a linear approximation, the state transition matrix for the time update of EKF is written as:

$$\boldsymbol{F}_k^{k+1} = \begin{pmatrix} \boldsymbol{I}_3 - \boldsymbol{\Omega}_e \tau_r & \boldsymbol{0} & \boldsymbol{0} & \boldsymbol{0} & \hat{\boldsymbol{C}}_b^e \tau_r \\ \boldsymbol{0} & \boldsymbol{I}_3 & \boldsymbol{I}_3 \tau_r & \boldsymbol{0} & \boldsymbol{0} \\ -(\hat{\boldsymbol{C}}_b^e \boldsymbol{f} \times)\tau_r & \boldsymbol{0} & \boldsymbol{I}_3 - 2\boldsymbol{\Omega}_e \tau_r & \hat{\boldsymbol{C}}_b^e \tau_r & \boldsymbol{0} \\ \boldsymbol{0} & \boldsymbol{0} & \boldsymbol{0} & \boldsymbol{I}_3 & \boldsymbol{0} \\ \boldsymbol{0} & \boldsymbol{0} & \boldsymbol{0} & \boldsymbol{0} & \boldsymbol{I}_3 \end{pmatrix} \tag{21}$$

By solving the EKF formulas with these equations, the rover antenna position and velocity are also obtained. In this case, the carrier-phase measurements of GPS/GNSS signals are not involved in these equations, so the cycle slips do not affect the solution.

INS/RTK-GPS INTEGRATION FOR CYCLE SLIP DETECTION AND FIXING

In this study, we employ a simple integration scheme of the RTK-GPS and INS/GPS solutions described in the previous sections. This INS/RTK-GPS integration scheme only replaces the time update step of EKF for RTK-GPS positioning expressed as equation (9) with:

$$\begin{aligned} \hat{\boldsymbol{r}}_{r,k+1}(-) &= \hat{\boldsymbol{r}}_{r,k}(+) + (\hat{\boldsymbol{v}}_{ins/gps,k+1} + \hat{\boldsymbol{v}}_{ins/gps,k})\tau_r / 2 \\ \hat{\boldsymbol{v}}_{r,k+1}(-) &= \hat{\boldsymbol{v}}_{ins/gps,k+1} \\ \boldsymbol{P}_{k+1}(-) &= \boldsymbol{F}_k^{k+1} \boldsymbol{P}_k(+) \boldsymbol{F}_k^{k+1^T} + \boldsymbol{Q}_k^{k+1} \end{aligned} \tag{22}$$

$$\boldsymbol{F}_k^{k+1} = \begin{pmatrix} \boldsymbol{I}_3 & & & \\ & \boldsymbol{0} & & \\ & & \boldsymbol{I}_{m-1} & \\ & & & \boldsymbol{I}_{m-1} \end{pmatrix}$$

$$\boldsymbol{Q}_k^{k+1} = \begin{pmatrix} \boldsymbol{P}_{v-ins/gps,k+1}\tau_r & & & \\ & \boldsymbol{P}_{v-ins/gps,k+1} & & \\ & & \boldsymbol{0} & \\ & & & \boldsymbol{0} \end{pmatrix}$$

where:

$\boldsymbol{P}_{v-ins/gps}$: covariance of INS velocity correction

In this scheme, the rover antenna position by the RTK-GPS process is projected to the next epoch with the corrected velocity by the INS/GPS integration process.

For the cycle slip detection, innovation tests are performed in the measurement update step of EKF for RTK-GPS. The innovation vector $\boldsymbol{\upsilon}$ and its covariance matrix $\boldsymbol{Q}_{\upsilon}$ at the epoch t_k are expressed as:

$$\begin{aligned} \boldsymbol{\upsilon} &= \boldsymbol{y}_k - \boldsymbol{h}(\hat{\boldsymbol{x}}_k(-)) \\ \boldsymbol{Q}_{\upsilon} &= \boldsymbol{H}(\hat{\boldsymbol{x}}_k(-))\boldsymbol{P}_k(-)\boldsymbol{H}(\hat{\boldsymbol{x}}_k(-))^T + \boldsymbol{R}_k \end{aligned} \tag{23}$$

The carrier-phase measurement is checked out as a potential cycle slip, if the square of its innovation exceeds the threshold with:

$$\upsilon_i^2 > n\, q_{i,\upsilon} \tag{24}$$

where υ_i is an innovation of $\boldsymbol{\upsilon}$, $q_{i,\upsilon}$ is the corresponding diagonal element of $\boldsymbol{Q}_{\upsilon}$ and n is the threshold factor usually set to 4 or 5.

Once potential cycle slips detected, using the projected rover antenna position aided by INS, the estimated carrier-phase ambiguity is reset to approximated values with:

$$N_{rb}^{ij} = \Phi_{rb}^{ij} - \rho_{rb}^{ij} \tag{25}$$

After that, the usual measurement update of EKF and ambiguity resolution processes for RTK-GPS run. The cycle slip is fixed through the process. This cycle slip detection and fixing can be applied to usual RTK-GPS algorithm without INS. It is, however, hard to provide good performance without INS because of the large variance of the predicted rover position.

FIELD EXPERIMENT

According to the procedure described above, we conducted an experiment to verify and evaluate the

performance of the proposed INS/RTK-GPS integration scheme.

Figure 4 shows the configuration of the field test. NovAtel GPS-702-GG antennas and OEMV-3 dual-frequency GPS receivers were employed for both of the rover and base-station. The rover antenna was mounted on the rooftop of a vehicle and connected to the receiver through a signal splitter. Additionally, to acquire the reference attitude of the vehicle, three sets of u-blox AEK-4T single-frequency GPS receivers were also installed. One output of the antenna splitter and two u-blox ANN-MS antennas, mounted on the left and right sides of the rooftop front, were connected to the u-blox receivers. All of the receivers' outputs were connected to a laptop PC via USB interfaces to record the raw GPS measurements at the sampling rate of 4 Hz. A low-cost MEMS-IMU device of Analog Devices ADIS16354 with tri-axis gyroscopes and accelerometers was fixed on the body of the vehicle. It was connected to the laptop PC via SPI/USB interface adapter as well. The PC sampled the raw measurement data of the IMU at the rate of 50 Hz. Figure 5 shows the snapshots of the field test. The compact MEMS-IMU device can be seen inside of the toolbox in the left picture. The right picture also shows the GPS antennas mounted on the rooftop of the vehicle. Table 1 shows the major specifications of the MEMS-IMU ADIS16354 used for the field test. The price of the device was about $700, that is reasonable as a factory-calibrated and temperature compensated MEMS-IMU.

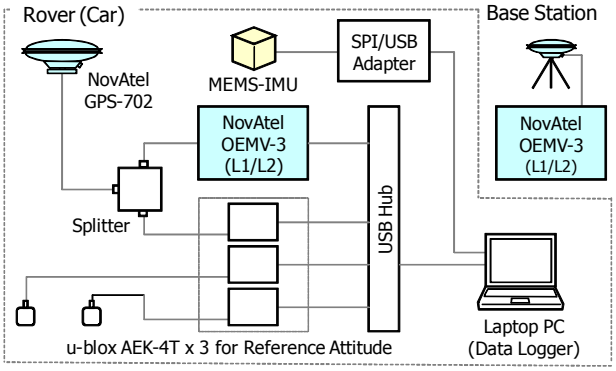

Figure 4. Configuration of field test


Figure 5. Snapshots of field test

Table 1. Specifications of ADIS16354

Item	Specification
Range	±300°/s, ±1.7g
Resolution	14-bits
Bandwidth	350 Hz
Gyroscope	
In Run Bias Stability	0.015°/s,
Angular Random Walk	4.2°/sqrt (hr)
Output Noise	0.60 °/s rms
Accelerometer	
Velocity Random Walk	0.135m/s/sqrt (hr)
Output Noise	4.7 mg rms
Factory Calibration	Sensitivity/Bias/Alignment
Temperature Sensor	Yes
Package Size	23 x 23 x 23 mm

As the field test, at first, we drove the vehicle with GPS receivers and IMU in the very good condition under the open sky with few obstacles along the path, to acquire the clear raw GPS measurements. Once the raw data obtained, we generated the reference trajectory by the post-mission kinematic baseline analysis with the raw GPS measurements of the vehicle in company with the base-station data. For the analysis, we used RTKLIB ver. 2.1.0, that is a precise GPS/GNSS positioning software package developed by the authors [6]. The time span of the reference trajectory was 7 minutes 30 seconds. The baseline length was from 0.0 to 0.9 km and the fix-rate was 100%. According to the variation at the stopping point, the relative accuracy of the reference trajectory would be below 1 cm as the horizontal RMS error.

After generating the reference trajectory, we added the artificial cycle slips to the raw carrier-phase measurements to simulate the situation in urban areas. The simulated slips were randomly generated weighted by the inverse of elevation angles. Figure 6 shows the three cases of these simulations: (1) with a few cycle slips, (2) with moderate cycle slips and (3) with extreme cycle slips. The number of the cycle slips for these cases were 81, 388 and 718, respectively.

The raw GPS data with the simulated cycle slips and the raw IMU data obtained by the field test were processed together according to the proposed INS/RTK-GPS integration scheme. The results were compared to the reference trajectory to evaluate the availability and accuracy. For comparison, the conventional RTK-GPS algorithm without INS was evaluated with the same GPS measurements. Figure 8-10 shows the trajectory and the position errors of the solutions for each case. In these figures, the green points are fixed solutions and the orange points indicate float solutions. Table 2 summarizes these results.

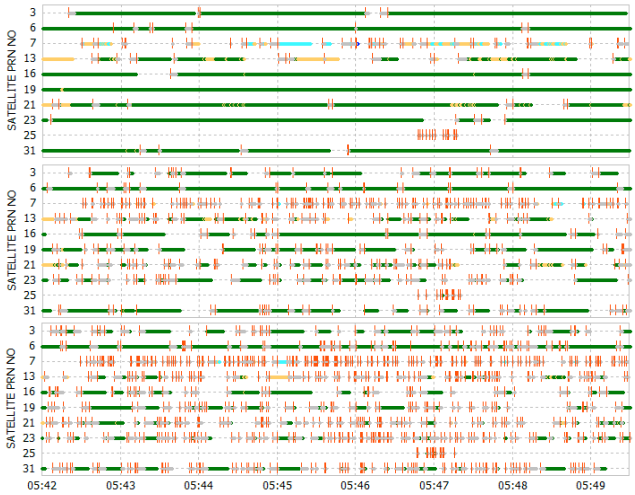

Figure 6. Simulated cycle slips (red lines). (1) with a few cycle slips (upper), (2) with moderate cycle slips (middle), (3) with extreme cycle slips (lower)

Table 2. Summary of results: availability (upper) and east/north/up RMS errors (cm) (lower) of fixed solutions

Case	Without INS			With INS		
(1) with a few cycle slips	92.9%			93.0%		
	0.3	0.4	0.5	0.3	0.4	0.6
(2) with moderate cycle slips	58.8%			64.5%		
	74.2	125.6	57.5	7.7	13.4	12.9
(3) with extreme cycle slips	28.4%			48.4%		
	346.6	573.4	306.4	16.2	24.3	26.3

As shown in Table 2, in the case with a few cycle slips, the INS/RTK-GPS integration shows almost same performance as without INS. The both cases indicate the high fix-rate and the cm-level accuracy. In the case with extreme cycle slips, however, with conventional RTK-GPS without INS, the fix-rate becomes very low and the accuracy is degraded over a few m level. The trajectory has many gaps and jumps. This degradation might be due to wrong fixed integer ambiguities. In contrast, integrated INS/RTK-GPS maintains higher fix-rate and better accuracy under a few 10 cm. The trajectory is smoother with INS. According to the results, especially in the severe condition, the proposed INS/RTK-GPS integration scheme works effectively to detect and fix the cycle slips. Figure 7 also shows the estimated attitude by the INS/RTK-GPS integration as the blue lines in the case with extreme cycle slips. Referenced to the attitude of red lines obtained by three GPS antennas and receivers, the RMS errors of roll, pitch and yaw angles are 1.01, 0.96 and 4.37 degree, respectively. With the proposed INS/RTK-GPS integration scheme, the attitude is also precisely determined even in the severe environment with many cycle slips.

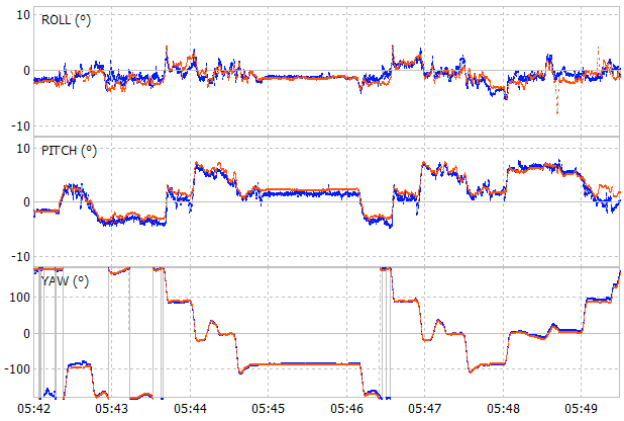

Figure 7. Estimated rover attitude (blue lines) and reference attitude (red lines) with extreme cycle slips

CONCLUSIONS AND FUTURE WORKS

To improve RTK-GPS performance for mobile vehicle navigation in urban areas, we focused on the issue of cycle slips. For cycle slip detection and fixing aided by INS, a simple integration scheme of INS/GPS and RTK-GPS is proposed. We conducted the field test to verify and evaluate the performance of the scheme. According to the experiments, the proposed scheme effectively works especially in the severe condition with many cycle slips. We need more experiments in more realistic situation with ill multipath environment. A direct integration of IMU measurements to the RTK-GPS filter, that is one of the potential improvements of the technique, should be investigated in the future study.

REFERENCES

[1] B.Hofmann-Wellenhof, H.Lichtenegger and J.Collins, Global Positioning System: Theory and Practice, Fifth, revised edition, SpringerWienNewYork, 2001

[2] A.Gelb ed., Applied Optimal Estimation, The M.I.T. Press, London, 1974

[3] P.J.G.Teunissen, The least-square ambiguity decorrelation adjustment: a method for fast GPS ambiguity estimation, J.Geodesy, vol.70, 1995

[4] X.-W.Chang, X.Yang and T.Zhou, MLAMBDA: A modified LAMBDA method for integer least-squares estimation, J.Geodesy, vol.79, 2005

[5] P.D.Groves, Principles of GNSS, Inertial, and Multisensor Integrated Navigation Systems, Artech House, Boston/London, 2008

[6] T.Takasu, N.Kubo and A.Yasuda, Development, evaluation and application of RTKLIB: A program library for RTK-GPS, GPS/GNSS symposium 2007, Tokyo, Japan, 20-22 November, 2007 (in Japanese)

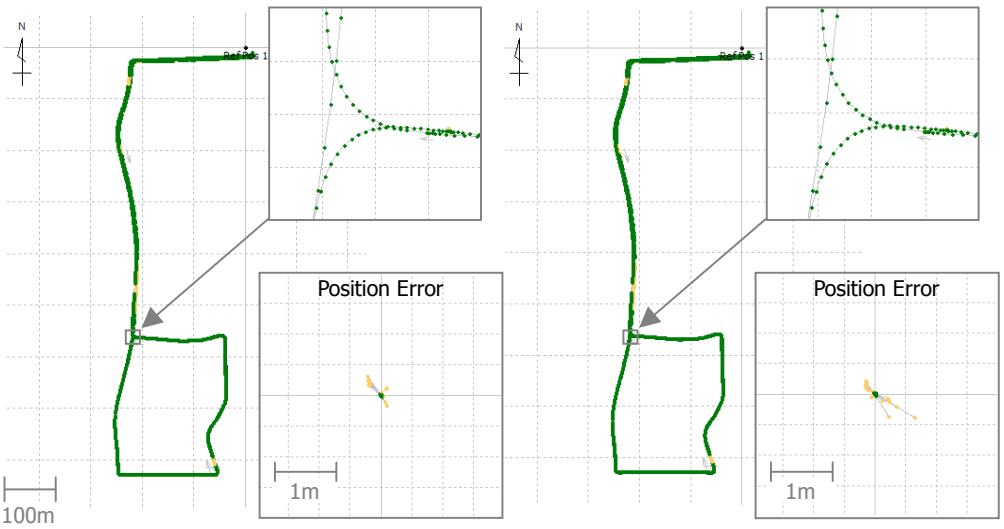

Figure 8. Trajectory and position errors (1) with a few cycle slips, without INS (left) and with INS (right)

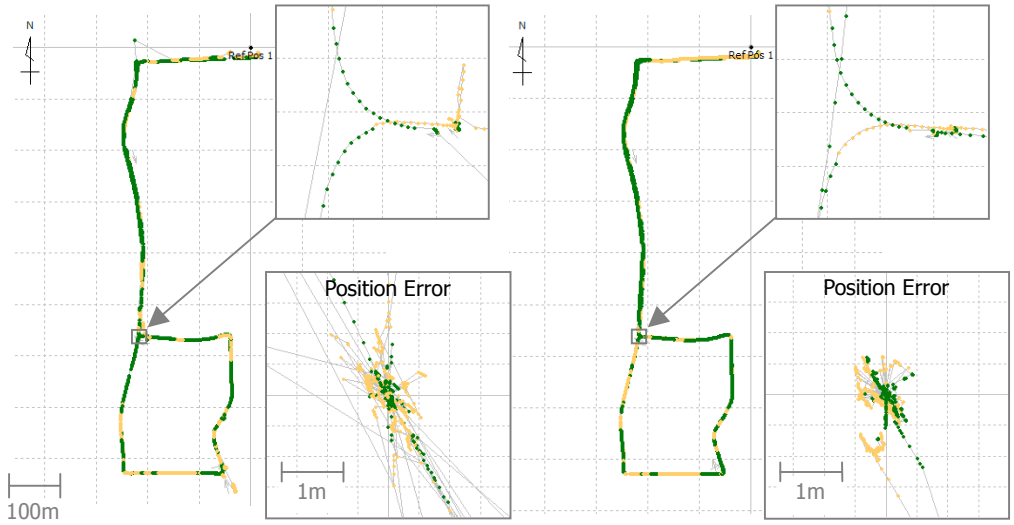

Figure 9. Trajectory and position errors (2) with moderate cycle slips, without INS (left) and with INS (right)

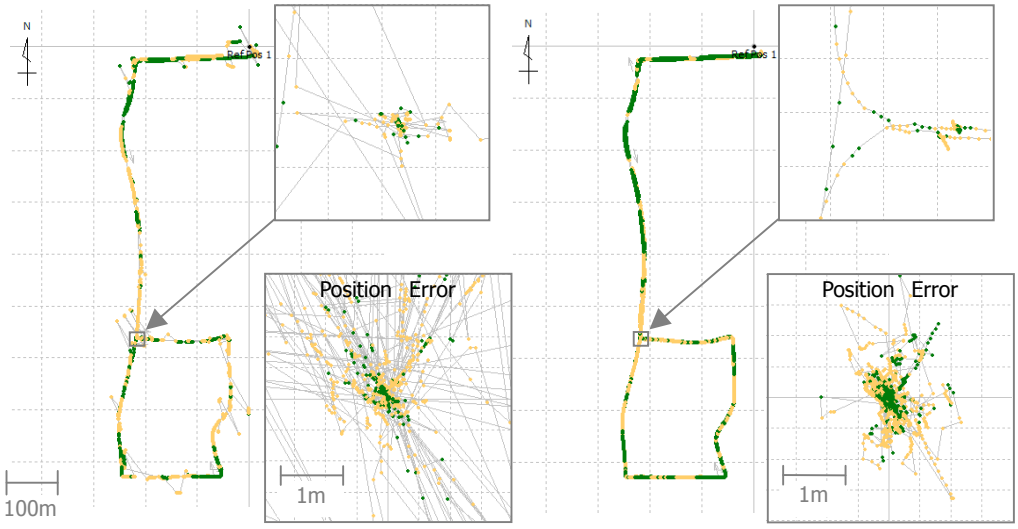

Figure 10. Trajectory and position errors (3) with extreme cycle slips, without INS (left) and with INS (right)